Original article

Nuclear Medicine Communications

Comparing approaches to correct for respiratory motion in NH_3 PET-CT cardiac perfusion imaging

Paul J. Schleyer, Michael J. O'Doherty, Sally F. Barrington, Geraint Morton and Paul K. Marsden

Aim **Respiratory motion affects cardiac PET-computed tomography (CT) imaging by reducing attenuation correction (AC) accuracy and by introducing blur. The aim of this study was to compare three approaches for reducing motion-induced AC errors and evaluate the inclusion of respiratory motion correction.**

Materials and methods **AC with a helical CT was compared with averaged cine and gated cine CT, as well as with a pseudo-gated CT, which was produced by applying PET-derived motion fields to the helical CT. Data-driven gating was used to produce respiratory-gated PET and CT images, and 60 NH_3 PET scans were attenuation corrected with each of the CTs. Respiratory motion correction was applied to the gated and pseudo-gated attenuation-corrected PET images.**

Results **Anterior and lateral wall intensity measured in attenuation-corrected PET images generally increased when PET-CT alignment improved and decreased when alignment degraded. On average, all methods improved PET-CT liver and cardiac alignment, and increased anterior wall intensity by more than 10% in 36, 33 and 25 cases for the averaged, gated and pseudo-gated CTAC PET images, respectively. However, cases were found where alignment worsened and severe artefacts resulted. This occurred in more cases and to a greater extent for the averaged and gated CT, where the anterior wall intensity reduced by more than 10% in 21 and 24 cases, respectively, compared with six cases for the pseudo-gated CT. Application of respiratory motion correction increased the average anterior and inferior wall intensity, but only 13% of cases increased by more than 10%.**

Conclusion **All methods improved average respiratory-induced AC errors; however, some severe artefacts were produced. The pseudo-gated CT was found to be the most robust method.** *Nucl Med Commun* **34:1174–1184** © **2013 Wolters Kluwer Health | Lippincott Williams & Wilkins.**

Nuclear Medicine Communications 2013, **34:**1174–1184

Keywords: PET-computed tomography, respiratory motion, respiratory motion correction

Division of Imaging Sciences and Biomedical Engineering, King's College London, King's Health Partners, St. Thomas' Hospital, London, UK

Correspondence to Paul J. Schleyer, PhD, Division of Imaging Sciences and Biomedical Engineering, King's College London, King's Health Partners, St. Thomas' Hospital, London SE1 7EH, UK
Tel: +44 20 7188 4988; fax: +44 20 7620 0790;
email: paul.schleyer@kcl.ac.uk

Received 6 June 2013 **Revised** 8 August 2013 **Accepted** 9 August 2013

Introduction

In dual-modality PET-computed tomography (CT) imaging, respiratory motion can produce two image-degrading effects. PET images are usually acquired over several respiratory cycles, resulting in motion-averaged images that contain blurring. The second effect is a result of the different temporal resolutions of PET and CT. In contrast to the long PET acquisition time, modern multislice CT scanners acquire helical CT (HCT) scans quickly (the lungs can be acquired in under 2 s), and each slice represents a snapshot of the respiratory cycle. Resulting spatial inconsistencies between PET and CT can lead to attenuation correction (AC) errors, particularly when regions of soft tissue are corrected with lower attenuation coefficients of lung [1].

In cardiac PET imaging, respiratory motion blurring in PET has been shown to create regions of significant heterogeneity in the myocardium [2]. In cardiac PET-CT imaging, AC errors resulting from respiratory motion have been identified as a source of artefacts that can resemble false defects [3], which can be severe when the PET-CT mismatch of the myocardium exceeds 8 mm [4,5]. Artefacts typically appear as reduced uptake in the anterior and lateral walls where a PET-CT misalignment of the myocardium exists; however, bias in septal [6] and inferior [5,7] walls can also occur from PET-CT misalignment of the liver.

Several approaches for reducing the effect of respiratory motion in cardiac PET-CT imaging exist. These are of varying degrees of complexity, and most can be generalized into three main categories. The first produces an AC map, which more closely matches the average respiratory position represented in the PET data. This can be achieved with breath-hold techniques [8–10], manually or automatically translating the CT to match the PET [4,11], acquiring a slow-rotation HCT [5,12], or acquiring a cine CT and averaging over the temporal

Data were presented at the SNM Annual meeting 2012 and published in abstract form.

0143-3636 © 2013 Wolters Kluwer Health | Lippincott Williams & Wilkins

DOI: 10.1097/MNM.0b013e328365bb27

dimension [13–15]. These approaches reduce respiratory-induced AC errors; however, motion blurring is not addressed.

In the second category, PET and cine CT images are respiratory gated, enabling matched AC in which each PET gate is attenuation-corrected with CT data from the matching point in the respiratory cycle [16–18]. This reduces AC errors that result from PET-CT misalignment. In addition, each PET gate produces a near motion-free image with reduced respiration motion blur. However, gating PET divides the acquired counts into several separate images, and this results in increased noise, which compromises the benefits of gating [19]. Summing the attenuation-corrected images produces a single image with reduced AC errors and with noise similar to the original, noncorrected PET image; however, motion blurring is reintroduced.

The third category reduces both motion blur and AC errors while maintaining image noise by motion correcting and recombining the matched attenuation-corrected PET data. This can be achieved either by reconstructing and then adding the gated images [20,21] or by including respiratory motion correction into iterative reconstruction methods [22–24].

As an alternative to using a gated cine CT for matched AC, a pseudo-gated CT can be generated by applying motion fields derived from gated PET images to a three-dimensional (3D) HCT volume. This approach has been demonstrated with thoracic images using nonlinear optical flow [25] and B-spline [26] registration. In cardiac PET-CT imaging, psuedo-gated CTs have been generated using rigid registration [27] and with respiratory models [28]. Pseudo-gated CTs offer an advantage over gated cine by reducing the dose; a 16 cm cine CT over the chest acquired using 140 kV, 10 mA and 5.5 s cine duration imposes a dose of $\sim$3 mSv, in contrast to $\sim$0.5 mSv resulting from an HCT of 8 mAs and 140 kV over the same region. In addition, the amplitude and period of respiration can vary from cycle to cycle [29–32], which can cause artefacts in gated cine CT [33]. Pseudo-gated CTs avoid this; however, they do rely on an artefact-free HCT that matches the respiratory position of one PET gate.

The aim of this study was to compare approaches that reduce cardiac NH_3 PET-CT misalignment-induced AC errors and motion-induced PET blurring. In particular, we determined which approaches are more likely to create, rather than reduce, respiratory motion artefacts in NH_3 cardiac PET-CT images. First, we evaluated approaches that reduce only AC artefacts: averaged cine CT (ACT), matched AC using gated cine CT and matched AC using pseudo-gated CT. These were compared with the standard approach of HCT-based AC. Following this, we evaluated the inclusion of respiratory motion correction with the matched AC images.

Materials and methods

Rest and stress NH_3 myocardial perfusion scans from 37 patients with known or suspected coronary artery disease were included in this study, and images were acquired on a GE Discovery VCT PET/CT scanner (General Electric Medical Systems, Waukesha, Wisconsin, USA). First, an HCT scan was acquired over 150 mm using 140 kVp, 20 mA, 0.4 s/rotation and a pitch of 1.375 : 1, and was reconstructed to 2.5-mm-thick slices. Following the HCT, patients were injected with $\sim$550 MBq of $^{13}NH_3$, and a 2D PET image was acquired for 26 min in listmode. The initial rapidly changing portion of NH_3 scans is not included in the relative assessment of myocardial perfusion [34], and for this work the 20 min of PET data obtained 6 min after injection were used. A cine CT image was then acquired at 140 kVp, 10 mA, 0.4 s/rotation, 5.5 s cine duration and 40 mm collimation, and was reconstructed to 2.5 mm contiguous slices. ECG gating was not used for PET or CT imaging.

Voluntary patient movement was determined by measuring the displacement of the spine between the helical scan and the cine CT scan, which were on average 30($\pm$4) min apart. In 14 cases, movement greater than 5 mm (approximately the resolution of PET) was measured, and these data sets were excluded from this study. The remaining 60 individual image data sets were analysed further. All patients consented to take part in the study, which was approved by a national ethics committee.

Respiratory gating

PET and cine CT acquisitions were respiratory gated using data-driven gating. The gating method used, which has been validated against a hardware-based gating method, derives a respiratory signal by observing the intensity change in the pixels, which are subject to respiratory motion throughout the acquisition [35,36]. PET and CT data were gated into eight gates. Variably sized amplitude gating was used to gate the PET data, in which the size (amplitude range) of each gate was adjusted such that an equal amount of acquisition time was assigned to each gate [37]. This ensured similar noise statistics in each sinogram gate.

Image registration

All nonrigid registrations used to create the pseudo-gated CT and for respiratory motion correction of PET were performed with NiftyReg version 1.3 (University College London, London, UK) [38]. This implements the B-spline-based free-form deformation method developed by Rueckert *et al.* [39], which uses normalized mutual information to determine image similarity at the voxel level. A 10 mm^3 final grid, 10 mm source and target filter, and a bending energy weight of 0.05 were used.

Attenuation-corrected PET data sets

Six attenuation-corrected PET image volumes were created for each scan, and these are summarized in Table 1. In method 1, the PET image attenuation-corrected with the HCT, AC_{HCT}, was used as the baseline for comparison. Methods 2–4 reduce AC artefacts only, and methods 5 and 6 reduce both AC artefacts and motion blur in PET by including registration. All PET reconstructions were performed with filtered back-projection using a 5.7 mm Hamming filter, 70 cm diameter and 293×293 slices.

(1) AC_{HCT}: The HCT was interpolated in the axial direction to match the positions of the PET slices before converting to CTAC. Gated PET sinograms were summed, attenuation-corrected, and reconstructed to create the AC_{HCT} PET volume.
(2) AC_{ACT}: All CT slices at each slice location of the 4D cine CT were averaged to create a single CT volume, which was interpolated in the axial dimension to match the PET position. Gated PET sinogram gates were summed, attenuation-corrected with the ACT and reconstructed to create the AC_{ACT} PET volume.
(3) AC_{GCT}: Each PET sinogram gate was attenuation-corrected with the CT gate with matching gate number. Gated attenuation-corrected PET data were then reconstructed and summed to create the single AC_{GCT} PET volume.
(4) AC_{pseudo}: A pseudo-cine CTAC was created by applying the motion fields derived from the non-attenuation-corrected (NAC) PET images to the helical CTAC image. First, the NAC PET gate that spatially matched the helical CTAC was identified by locating the superior edge of the liver in both data sets (described below), and the PET gate with the closest liver position to the helical CTAC was defined as the matching gate. This matching NAC PET gate was registered to each remaining NAC PET gate, creating seven transformations that were then applied to the helical CTAC. This produced a CTAC for each respiratory position represented by the gated PET series, effecting the pseudo-gated CT sequence. PET sinograms were attenuation-corrected with the matching pseudo-gated CT gate, reconstructed, and summed to create the single AC_{pseudo} PET volume.
(5) $ACReg_{GCT}$: Gated PET sinograms were attenuation-corrected with matching CT gates as for method 3, and individually reconstructed. All PET image gates were registered to the expiration gate, which was assumed to be the gate with the most superior centre of mass. To avoid compounding the effects of any remaining spatial misalignment between PET and AC maps, motion correction transformations were derived from gated, NAC PET images, and the transformations were applied to the attenuation-corrected images. Following registration, all attenuation-corrected PET gates were summed.
(6) $ACReg_{pseudo}$: The same procedure as applied for method 5 was carried out, except for the use of pseudo-gated CT rather than gated cine CT.

Evaluation

The six respiratory motion correction approaches (methods 1–6) were evaluated in two separate stages. First, the different AC methods (methods 1–4) were compared using two metrics: PET-CT alignment and relative difference in myocardial wall intensities in attenuation-corrected short-axis (SA) PET images. In the second stage, the effects of implementing registration (methods 5 and 6) were evaluated.

Attenuation correction

First, alignment between the NAC PET images and each CTAC was assessed to compare the four approaches of AC (methods 1–4). Liver and myocardium positions in each NAC PET and CTAC gate were determined from profiles over each organ (described below). Alignment was defined as the absolute difference between NAC PET and CT positions averaged over all gates. For the gated and pseudo-gated CTs, each NAC PET gate was compared with the matching CTAC gate, and for the averaged cine and HCT each NAC PET gate was compared with the single static CT.

Second, the four AC methods were compared by measuring the myocardium intensity in the attenuation-corrected images AC_{HCT}, AC_{ACT}, AC_{GCT} and AC_{pseudo}. The AC PET image volumes were rotated to create SA slices, which were smoothed with a 3D Gaussian 4.8 mm FWHM filter to reduce image noise and allow for direct comparison of volumes. Two profiles, one towards the base and one towards the apex, were manually defined on each of the anterior, inferior, lateral and septal walls of the

Table 1 Summary of the six AC PET images created for each study

Method	CTAC	PET	Attenuation correction	Single resulting image
1. AC_{HCT}	Helical	Nongated	Nonmatched	Summed
2. AC_{ACT}	Average cine	Nongated	Nonmatched	Summed
3. AC_{GCT}	Gated cine	Gated	Matched	Summed
4. AC_{pseudo}	Pseudo-gated	Gated	Matched	Summed
5. $ACReg_{GCT}$	Gated cine	Gated	Matched	Registered and summed
6. $ACReg_{pseudo}$	Pseudo-gated	Gated	Matched	Registered and summed

Respiratory motion correction was performed on gated and pseudo-gated CT-corrected PET images.
AC, attenuation correction; ACT, averaged cine CT; CT, computed tomography; HCT, helical CT.

SA slices. For each acquisition, one set of profiles was defined and copied onto all AC image data sets. The peak of each profile was used to indicate cardiac wall intensity.

As the true myocardial activity is unknown, relative change in myocardial intensity was used to evaluate AC methods 2–4, using the AC_{HCT} images as the baseline for comparison. When poor PET-CT alignment exists, the anterior wall of the myocardium in PET can correspond to the lung in the CT, and this can result in undercorrection for attenuation and reduced activity in the attenuation-corrected PET image. Replacing this CT with a CT that improves alignment is therefore expected to increase anterior wall intensity in the AC PET images. Conversely, a decrease in anterior wall intensity in AC PET would result if the replacement CT worsens PET-CT alignment. A positive correlation between the change in PET-CT alignment and change in anterior wall activity is therefore expected.

Respiratory motion correction

The range of liver and cardiac motion was determined by measuring the liver and myocardial edge (described below) on the NAC-gated PET image series on both the motion corrected and non-motion-corrected images. Accuracy of respiratory motion correction was indicated by the reduction in motion range.

The effect of applying respiratory motion correction was also determined by evaluating the change in myocardial wall intensity in attenuation-corrected PET images. Profiles were defined over the myocardium on SA images $ACReg_{GCT}$ and $ACReg_{pseudo}$, and on the nonregistered SA images (rigid body registration was first used to align the ACReg images with the AC images such that the profile locations copied onto all data sets represented corresponding anatomical positions). AC_{GCT} and AC_{pseudo}, and the change in cardiac wall intensity, described the effect of applying respiratory motion correction. As respiratory motion can blur the myocardial wall and effectively reduce the wall intensity, an increase in wall intensity is expected when motion blurring is reduced.

Liver and myocardial edge

The location of the liver and myocardium along the z-axis in PET and CT images was necessary to match the HCT with the gated PET (to produce the pseudo-gated CT) and to evaluate PET-CT alignment. To determine the position of these organs, profiles of the superior edges of the liver and myocardium were obtained by projecting a volume of interest defined over the organ edge onto the z-axis. To reduce profile noise in the PET images, a further 4 mm Gaussian filter was applied before defining the volumes of interest.

A straight line was fitted to the central segment of the profile, which spanned 20–80% of the profile range. The point where the fitted line intercepted 50% of the profile range defined the approximate location of the organ edge along the z-axis. Figure 1 illustrates the liver edge definition for PET and CTAC slices from the same patient. The displacement between the liver positions in PET and CTAC is highlighted.

Results

Averaged, gated and pseudo-gated CTs were generated for all acquisitions. In 45 of the 60 scans, the pseudo-gated CT produced a larger range of myocardium respiratory motion compared with the gated cine. On average, the range of liver and myocardium respiratory

Fig. 1

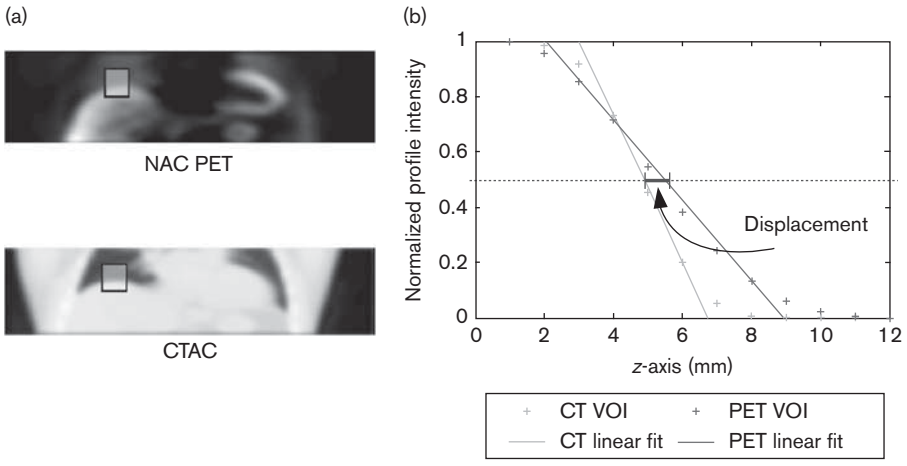

PET-CT alignment of the liver. A profile was defined along the z-axis over the liver edge in both data sets, and a straight line was fitted to the section ranging from 0.8 to 0.2 of the intensity normalized profile. Alignment was defined as the z-axis separation between the two straight lines at $y=0.5$. CT, computed tomography; NAC, non-attenuation-corrected; VOI, volume of interest.

motion measured in the pseudo-gated CT was 13.1 and 6.9 mm, respectively, significantly greater than the average motion measured on the gated cine, which was 7.6 and 4.9 mm, respectively.

Attenuation correction

PET-CT alignment

On observing the overall PET-CT alignment for all scans, we found that the pseudo-gated CT produced the best liver and cardiac alignment, with a mean alignment of 1.9 and 5.4 mm, respectively. The HCT produced the worst liver and cardiac alignment, with 5.2 and 6.5 mm, respectively.

Compared with the HCT, the ACT, GCT and pseudo-gated CT all improved the mean PET-CT alignment of the liver and myocardium, as shown in Table 2. Only the pseudo-gated CT demonstrated a significant improvement of both the liver and the myocardium. All three cine CTs also produced cases in which cardiac wall alignment was worse when compared with the HCT. The pseudo-gated CT produced the smallest degrading effect, up to 3.2 mm, whereas the alignment worsened by up to 9.6 and 11.2 mm for the average and gated cine CTs, respectively.

Cardiac wall intensity

Using the HCT as a baseline for comparison, the SA PET images AC_{ACT}, AC_{GCT} and AC_{pseudo} were compared with the AC_{HCT} images to observe the relative change in myocardial wall intensity. The PET images of two example patients are shown in Fig. 2. In Fig. 2a, the ACT, GCT and pseudo-gated CT are all seen to improve the alignment when compared with the HCT. An anterior apical wall defect apparent in the AC_{HCT} PET image is not present in the AC_{ACT}, AC_{GCT} and AC_{pseudo} PET images. For this case, the mean liver and cardiac wall PET-CT misalignment was reduced from 10.6 and 7.9 mm, respectively, when the HCT was used to 2.7 and 3.0 mm for the GCT and 4.7 and 0.6 mm for the pseudo-gated CT, respectively.

In the second example, Fig. 2b, the ACT and GCT both produced worse cardiac PET-CT alignment (9.9 and 11.5 mm, respectively) compared with the HCT (0.3 mm) and pseudo-gated CT (1.6 mm). A spatial PET-CT misalignment for ACT and GCT results in an artefact that appears as an anterior wall defect and is seen in the AC_{GCT} PET image but not in the AC_{HCT} PET image. A 37% decrease in anterior wall intensity was found with the AC_{GCT} PET data. The AC_{pseudo} PET images were not visually different from the AC_{HCT} images.

Table 2 Mean±SD improvement (mm) in liver and myocardial wall PET-CT alignment (no motion correction) using the HCT as a baseline for comparison

	Alignment improvement (mm)		
	AC_{ACT}	AC_{GCT}	AC_{pseudo}
Liver	1.3 (±4.8)*	0.9 (±5.2)	3.3 (±2.7)*
Myocardium	0.9 (±3.7)	0.3 (±3.9)	1.1 (±2.5)*

AC, attenuation correction; ACT, averaged cine CT; CT, computed tomography; HCT, helical CT.
*Significant ($P<0.05$).

The mean change in intensity of the SA walls for all patients is shown in Table 3. In Fig. 3, the change in anterior and lateral cardiac wall intensities is shown as histograms, in which more of a positive bias can be seen for the AC_{pseudo} PET images. The AC_{ACT} and AC_{GCT} PET images showed more cases of a large decrease in intensity. A decrease in anterior wall intensity of more than 10% was seen in 21 and 24 cases in the AC_{ACT} and AC_{GCT} PET images, respectively, compared with only six cases in the AC_{pseudo} images. However, slightly fewer cases were found when the anterior wall increased by more than 10% in the AC_{pseudo} images: 25 cases compared with 36 and 33 cases in the AC_{ACT} and AC_{GCT} images, respectively.

The septal and inferior walls were less affected; however, an increase of up to 22% and a decrease of up to 39% were found. No correlation was found between the change in inferior wall intensity and the change in cardiac wall alignment; however, a correlation was found with liver alignment ($P < 0.001$). Similarly for the septal wall, a higher correlation with wall intensity change was found with liver alignment than with cardiac alignment. When the pseudo-gated CT improved alignment by reducing a superior displacement of the liver, the inferior and septal wall intensity decreased by more than 10% in 13 cases, suggesting overcorrection of attenuation in the septal and inferior walls by superior displacement of the liver with the HCTs.

The change in anterior wall intensity was well correlated with the change in PET-CT cardiac alignment ($\rho = 0.72$, $P < 0.001$), and, in general, the anterior wall intensity increased when alignment improved and decreased when the alignment was poor. Figure 4 shows the percentage change in anterior wall intensity and the change in alignment for each anterior wall SA measurement.

Exceptional cases were noted on the gated and averaged cine data sets, in which an increase in anterior wall intensity of more than 10% resulted from a worse PET-CT alignment. In these cases, motion artefacts in the gated and average cine CTs produced a spatial discontinuity along the anterior wall, and the alignment measurement did not accurately represent the PET-CT displacement at the apical section of the anterior wall. In one case, an improvement in PET-CT alignment resulted in a decrease in anterior wall intensity of $\sim$20%. In this case, the myocardium position in the HCT was superior to the position in PET. Although the absolute PET-CT alignment improved when the ACT and GCT were used, the myocardium position in these CTs was up to 10 mm

Fig. 2

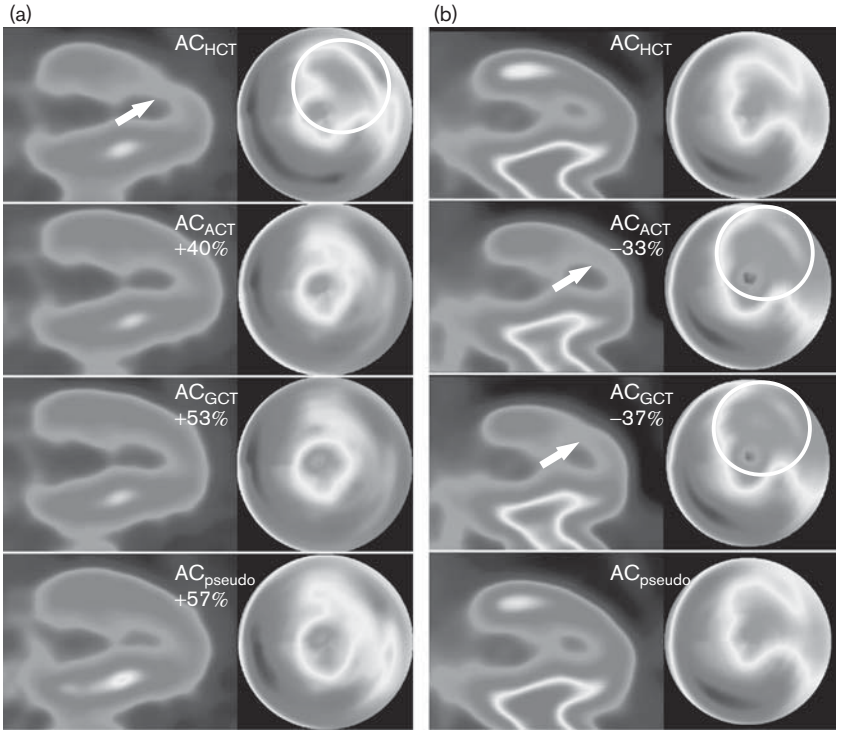

(a) Example 1. (b) Example 2. Bullseye and horizontal long-axis images of two example cases. (a) An artefact that resembles a defect on the anterior wall is seen on the AC_{HCT} PET images, which results from a PET-CT spatial mismatch. This artefact is corrected in AC_{ACT}, AC_{GCT} and AC_{pseudo} images from improved PET-CT alignment. (b) Good PET-CT alignment exists for the AC_{HCT} and AC_{pseudo} data sets, and no defect is seen. For the AC_{ACT} and AC_{GCT} images, worse PET-CT alignment produces an artefact that appears as an anterior wall defect. AC, attenuation correction; ACT, averaged cine CT; CT, computed tomography; HCT, helical CT; NAC, non-attenuation-corrected.

Table 3 Mean±SD change (%) in SA wall intensities using AC_{HCT} as a baseline for comparison

	Intensity change (%)				
SA wall	AC_{ACT}	AC_{GCT}	AC_{pseudo}	$ACReg_{GCT}$	$ACReg_{pseudo}$
Anterior	4.8 (±20.0)*	3.0 (±20.5)	3.9 (±11.3)*	6.9 (±21.5)*	8.6 (±14.0)*
Inferior	−4.5 (±9.2)*	−4.8 (±9.1)*	1.5 (±3.9)*	−0.4 (±10.7)	6.3 (±7.4)*
Septal	0.0 (±9.1)	−0.5 (±9.3)	2.1 (±4.5)*	0.7 (±10.2)	3.4 (±6.0)*
Lateral	−1.2 (±15.0)	−1.9 (±14.9)	2.8 (±8.3)*	−2.4 (±14.9)	3.6 (±9.4)*

AC, attenuation correction; ACT, averaged cine CT; CT, computed tomography; HCT, helical CT; SA, short axis.
*Significant ($P<0.05$).

inferior to the PET position in some gates, resulting in an undercorrection of the anterior wall.

Respiratory motion correction

The range of respiratory motion was measured on the gated NAC PET images before and after respiratory motion correction. On average, the range of liver motion reduced from 12.2 to 1.0 mm, and the cardiac wall respiratory motion range reduced from 8.3 to 0.8 mm.

Application of respiratory motion correction to the AC_{GCT} and AC_{pseudo} PET images significantly increased the intensity of all SA walls ($P < 0.05$), with the largest change seen in the anterior and inferior walls, as shown in Table 4. The change in wall intensity was significantly correlated with total respiratory motion range for the anterior and inferior walls ($P < 0.001$); however, no correlation was found for the septal and lateral walls. This is demonstrated in Fig. 5, which shows the change in cardiac wall intensities measured on $ACReg_{GCT}$ and $ACReg_{pseudo}$ images, with respect to the total respiratory-induced displacement range measured on NAC PET images.

In 13% of cases, the nonrigid correction increased the anterior wall intensity by 10% or greater. Figure 6 shows representative SA slices for a case in which respiratory motion correction increased the anterior wall intensity by 26% for the AC_{GCT} images and by 28% for the AC_{pseudo} images.

Fig. 3

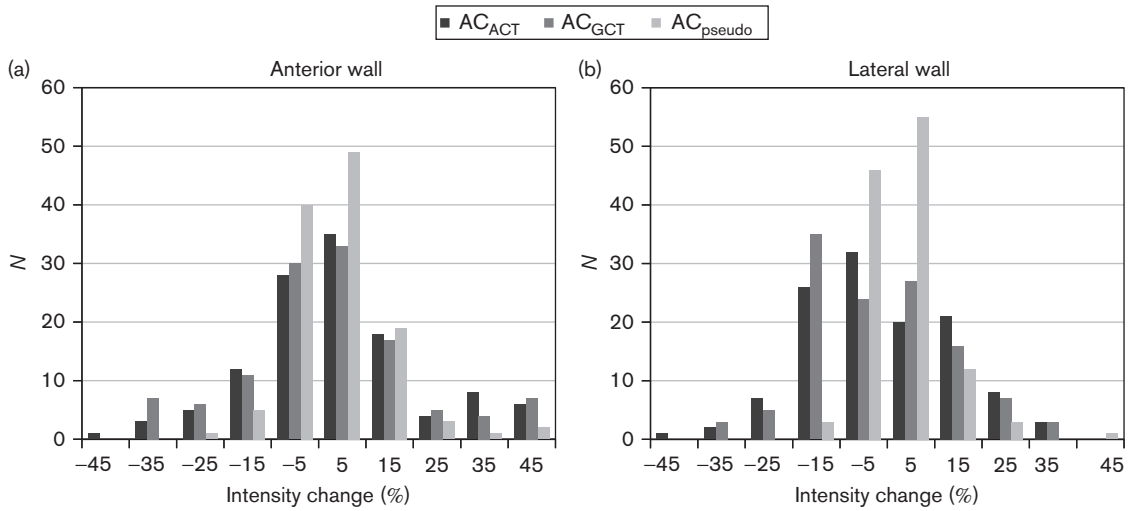

The percentage change in cardiac (a) anterior and (b) lateral wall intensities in PET images when the helical CTAC was replaced with the average, gated and pseudo-gated CTACs. More of a positive bias is seen with the AC_{pseudo} images. AC, attenuation correction; ACT, averaged cine CT.

Fig. 4

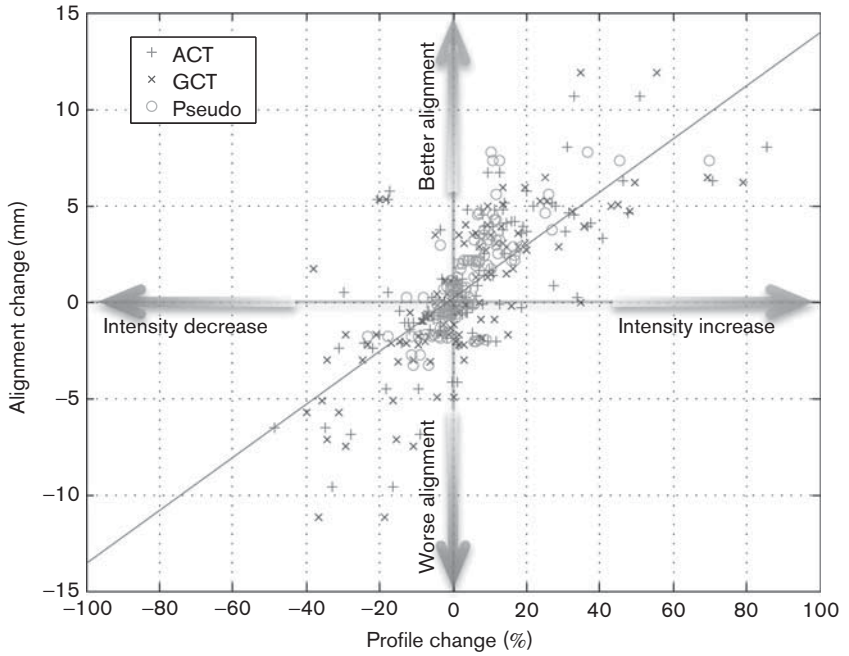

The change in both PET-CT alignment and anterior wall intensity that results from replacing the HCT with the ACT, GCT or pseudo-gated CT. Generally, an improvement in alignment (a positive change) creates an increase in anterior wall intensity, and a worse alignment (a negative change) produces a decrease in anterior wall intensity. The solid diagonal line indicates linear fit of all data ($y = 0.14x + 0.21$). ACT, averaged cine CT; CT, computed tomography; HCT, helical CT.

When compared with the AC_{HCT} images, an anterior wall intensity increase of greater than 10% was seen in 14% and 23 of cases for the $ACReg_{GCT}$ and $ACReg_{pseudo}$ images, respectively.

Discussion

PET-CT misalignment can lead to AC errors, which in cardiac imaging can present as false defects. Compared with the HCT, the ACT, GCT and pseudo-gated CTs, on

Table 4 Average change (%) in SA wall intensities resulting from respiratory motion correction

	Intensity change (%)	
SA wall	$ACReg_{GCT}$	$ACReg_{pseudo}$
Anterior	4.0 (±6.0)*	4.4 (±5.26)*
Inferior	4.6 (±4.7)*	4.7 (±4.8)*
Septal	1.3 (±3.9)*	1.3 (±3.8)*
Lateral	−0.4 (±3.1)*	0.7 (±3.3)*

SA, short axis.
*$P<0.05$.

Fig. 5

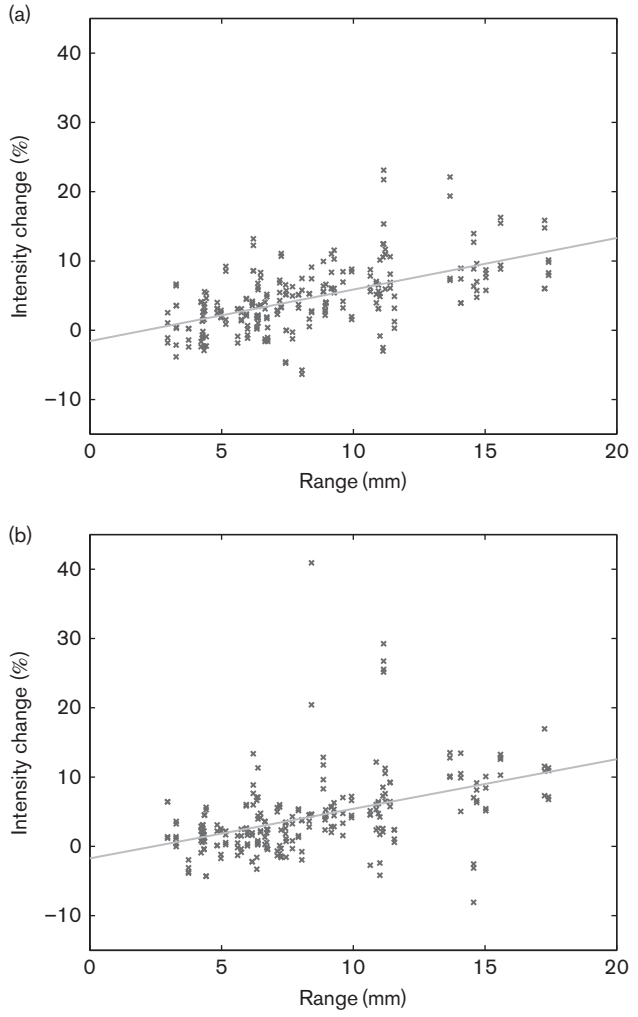

For the anterior (a) and inferior (b) walls, a significant ($P<0.05$) correlation was found between the effect of respiratory motion correction (the change in profile maximum measured on $ACReg_{GCT}$ and $ACReg_{pseudo}$) and the range of respiratory-induced motion measured on NAC-gated PET images. No correlation was found for the septal and lateral walls. NAC, non-attenuation-corrected.

average, improved the liver and cardiac PET-CT alignment. Importantly, however, all methods were also shown to worsen the alignment in some cases. As a consequence of worse alignment, the ACT decreased the anterior wall intensity in AC PET images by more than 10% in 21 out of 60 cases, which is comparable to findings from other groups; Alessio *et al.* [15] found that in 23% of cases the ACT produced unacceptable PET-CT alignment, and Gould *et al.* [5] found artefactual defects in both HCT and ACT data sets in 19% of cases.

A high correlation between the change in cardiac PET-CT alignment and the change in wall intensity was found for the anterior and lateral walls. PET-CT misalignment of these walls is expected to locally reduce the intensity in AC PET images, as undercorrection of attenuation results from replacing myocardium μ values with smaller lung μ values. No cases were found that suggested overcorrection of the lateral and anterior walls, in which a superior displacement of the myocardium would increase anterior or lateral wall intensity. We can therefore assume that an increase in the intensity of the lateral and anterior walls reflects an improvement in accuracy, and a decrease indicates a loss of accuracy.

A significant decrease in inferior wall intensity was found for the AC_{ACT} and AC_{GCT} data; however, a small but significant increase was found for the AC_{pseudo} data. Misalignment of the liver is known to affect the inferior wall, and the pseudo-gated CT produced the best liver alignment. All three cine CTs demonstrated cases in which liver alignment worsened, by up to 13.1 mm for the ACT and GCTs; however, for the pseudo-gated CT the largest degradation of alignment was only 1.6 mm. Additional to liver alignment, we also observed that PET-CT misalignment can result in incorrect AC of the inferior wall with fat, and this could contribute to the reduction in inferior wall activity seen in AC_{ACT} and AC_{GCT} images with poorer PET-CT alignment.

A degradation of alignment and resulting decrease in anterior wall intensity occurred in more cases and to a greater extent when the HCT was replaced with the ACT and GCT, compared with the pseudo-gated CT, which produced fewer and less severe cases. Conversely, when the alignment improved and the intensity of the anterior wall increased as a result, the ACT and GCT had a greater effect than the pseudo-gated CT. This is reflected in the 21 cases in which the AC_{ACT} PET images produced more than 10% increase in anterior wall intensity when compared with AC_{pseudo}.

Of the AC methods evaluated in this study, the pseudo-gated CT was found to be the most robust. Regardless of the AC approach used, visual assessment of PET-CT alignment appears necessary as misalignment can still exist. In addition, images that demonstrated voluntary motion were excluded from this study, further highlighting this requirement.

Despite the significant correlation between the effect of respiratory motion correction and the range of respiratory-induced displacement, the cases in which respiratory

Fig. 6

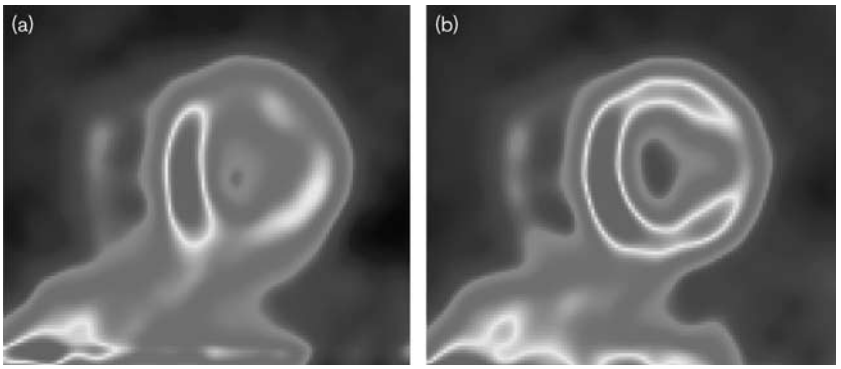

Short-axis slices for the (a) nonregistered AC_{GCT} and (b) registered $ACReg_{GCT}$ PET images. Motion correction increased the anterior and inferior wall maximum by 26 and 19%, respectively. AC, attenuation correction.

motion correction produced the largest change in inferior and anterior wall intensity were not necessarily the cases with the largest motion range. A likely explanation for this is the variation in respiratory characteristics between patients, as both the amplitude of motion and the amount of acquisition time spent at maximum displacement will determine the effect of motion in the PET image. Liu *et al.* [40] found that PET images of patients who spent a large portion of the respiratory cycle at expiration phase were less affected by respiratory motion than were images of patients with irregular breathing patterns. In our study, respiratory motion correction did generally produce a smaller average effect when a large portion of time was spent at expiration; however, exceptions to this were found. Additional factors could explain this, including differences in myocardial wall thickness and the residual blurring in PET gates. Moreover, a variable amplitude-gating method was used that produces gates of equal noise, and a potential consequence of this is increased motion blurring in some gates.

The findings of this study are confined to the specific methods of respiratory motion reduction used. Simple approaches to each concept were implemented, and improvements to each of the methods may alter the results. Average cine CT was chosen, as this is the method currently available on the scanner used in this work; however, a maximum intensity projection cine CT has been shown to produce superior results [15]. Cine CT images were gated with a data-driven gating method, and the AC_{GCT} PET images were similar to the AC_{ACT} images. An improvement to the gating could improve PET-CT misalignment, and hardware gating methods or other data-driven CT gating methods may produce superior results [41–45]. Finally, the pseudo-gated CT was derived in a simple manner by applying PET-derived motion fields to the HCT. McQuaid *et al.* [28] have produced a detailed method of generating cine CTs from static CT images, and Alessio *et al.* [46] have shown that consistency criteria can also be used to reduce respiratory motion artefacts in cardiac PET imaging. These approaches may improve the results for the pseudo-gated CT approach.

Limitations of the methods used for measuring the PET-CT misalignment and measuring cardiac wall profiles must also be considered. Measuring the edge of an object in a PET image is not well defined because of resolution effects, and in this work the edge was approximated as the midpoint between the local minimum and maximum on either side of the edge. This could be a source of error in the PET-CT misalignment values; however, the results demonstrate that, generally, the relative change in cardiac wall measurement approached zero as the PET-CT misalignment approached zero, supporting the accuracy of the approximation. Alignment was, however, only calculated at one position on the myocardial wall and liver, which may not truly represent the alignment throughout the entire area of interest, and cases were found in which the alignment at the basal region did not represent alignment at the apical region. Similarly, only eight cardiac wall profiles were measured, and some changes in the myocardium may have been undetected.

Respiratory motion correction did not degrade image quality (by reducing cardiac wall intensity by >10%), and when correcting the AC_{pseudo} and AC_{GCT} PET images for respiratory motion 13% of anterior wall profiles increased by more than 10%. This seems low; however, only the effect of blurring has been considered. On correcting for both PET-CT mismatch and blurring (by comparing $ACReg_{pseudo}$ to AC_{HCT}), we found that the anterior wall intensity increased by more than 10% in 23% of cases.

This implementation of respiratory motion correction could potentially improve; gated and reconstructed images were individually registered to the expiration gate and summed to create the motion-corrected image. Other registration methods such as optical flow [21],

combining the registration within iterative reconstruction [22–24,47,48] and combining the generation of a pseudo-gated CT with registration and reconstruction [49] all potentially improve the results.

Conclusion

In general, more accurate AC by improving cardiac PET-CT alignment increased the anterior and lateral cardiac wall intensity measured on AC PET, and worse PET-CT alignment, resulting in less accurate AC, decreased the intensity of these walls. The inferior and septal walls were prone to both overcorrection and undercorrection for attenuation. Compared with the standard approach of using an HCT for AC, on average, all three methods of reducing respiratory motion-induced AC errors improved PET-CT alignment and increased the anterior wall intensity. However, all three methods also produced cases in which alignment worsened, and in some cases a severe artefact appearing as a defect resulted. This occurred in more cases and to a greater extent for the ACT and GCT methods, and the pseudo-gated cine CT was found to be the most robust method for reducing respiratory-induced AC artefacts in NH_3 cardiac PET-CT imaging.

Respiratory motion correction generally increased the inferior and anterior wall intensity, and the amount of change was correlated with the range of respiratory motion. Although respiratory motion correction produced a large effect only in a small number of cases, up to 41% change in anterior wall intensity was demonstrated. Furthermore, no degrading effects were found when respiratory motion correction was applied.

Acknowledgements

This paper presents independent research commissioned by the National Institute for Health Research (NIHR) under its Invention for Innovation (i4i) Programme (NEAT). The views expressed are those of the authors and not necessarily those of the NHS, the NIHR or the Department of Health.

Conflicts of interest

There are no conflicts of interest.

References

1 Osman MM, Cohade C, Nakamoto Y, Wahl RL. Respiratory motion artifacts on PET emission images obtained using CT attenuation correction on PET-CT. *Eur J Nucl Med Mol Imaging* 2003; **30**:603–606.

2 Ter-Pogossian MM, Bergmann SR, Sobel BE. Influence of cardiac and respiratory motion on tomographic reconstructions of the heart – implications for quantitative nuclear cardiology. *J Comput Assist Tomogr* 1982; **6**:1148–1155.

3 Le Meunier L, Maass-Moreno R, Carrasquillo JA, Dieckmann W, Bacharach SL. PET/CT imaging: effect of respiratory motion on apparent myocardial uptake. *J Nucl Cardiol* 2006; **13**:821–830.

4 Martinez-Möller A, Souvatzoglou M, Navab N, Schwaiger M, Nekolla SG. Artifacts from misaligned CT in cardiac perfusion PET/CT studies: frequency, effects, and potential solutions. *J Nucl Med* 2007; **48**:188.

5 Gould KL, Pan T, Loghin C. Frequent diagnostic errors in cardiac PET/CT due to misregistration of CT attenuation and emission PET images: a definitive analysis of causes, consequences, and corrections. *J Nucl Med* 2007; **48**:1112–11121.

6 McQuaid SJ, Hutton BF. Sources of attenuation-correction artefacts in cardiac PET/CT and SPECT/CT. *Eur J Nucl Med Mol Imaging* 2008; **35**:1117–1123.

7 Chin BB, Nakamoto Y, Kraitchman DL, Marshall L, Wahl R. PET-CT evaluation of 2-deoxy-2-[^{18}F] fluoro-D-glucose myocardial uptake: effect of respiratory motion. *Mol Imaging Biol* 2003; **5**:57–64.

8 Goerres GW, Kamel E, Seifert B, Burger C, Buck A, Hany TF, *et al.* Accuracy of image coregistration of pulmonary lesions in patients with non-small cell lung cancer using an integrated PET/CT system. *J Nucl Med* 2002; **43**:1469–1475.

9 Goerres GW, Kamel Ehab, Thai-Nia H. PET-CT image co-registration in the thorax: influence of respiration. *Eur J Nucl Med Mol Imaging* 2002; **29**: 351–360.

10 Beyer T, Antoch G, Blodgett T, Freudenberg LF, Akhurst T, Mueller S. Dual-modality PET/CT imaging: the effect of respiratory motion on combined image quality in clinical oncology. *Eur J Nucl Med Mol Imaging* 2003; **30**:588–596.

11 Khurshid K, McGough RJ, Berger K. Automated cardiac motion compensation in PET/CT for accurate reconstruction of PET myocardial perfusion images. *Phys Med Biol* 2008; **53**:5705–5718.

12 Nye JA, Esteves F, Votaw JR. Minimizing artifacts resulting from respiratory and cardiac motion by optimization of the transmission scan in cardiac PET/CT. *Med Phys* 2007; **34**:1901–1906.

13 Cook R, Carnes G, Lee T-Y, Wells RG. 4D CT for respiratory gated attenuation corrections in canine cardiac PET imaging. In: IEEE Nuclear Science Symposium Conference Record; 16–22 October 2004; Rome, Italy. Vol. 4. pp. 2408–2412.

14 Pan T, Mawlawi O, Luo D, Liu HH, Chi P-CM, Mar MV, *et al.* Attenuation correction of PET cardiac data with low-dose average CT in PET/CT. *Med Phys* 2006; **33**:3931–3938.

15 Alessio AM, Kohlmyer S, Branch K, Chen G, Caldwell J, Kinahan P. Cine CT for attenuation correction in cardiac PET/CT. *J Nucl Med* 2007; **48**: 794–801.

16 Nehmeh SA, Erdi YE, Pan T, Pevsner A, Rosenzweig KE, Yorke E, *et al.* Four-dimensional (4D) PET/CT imaging of the thorax. *Med Phys* 2004; **31**: 3179–3186.

17 Nagel CCA, Bosmans G, Dekker aLAJ, Öllers MC, De Ruysscher DKM, Lambin P, *et al.* Phased attenuation correction in respiration correlated computed tomography/positron emitted tomography. *Med Phys* 2006; **33**:1840–1847.

18 Pönisch F, Richter C, Just U, Enghardt W. Attenuation correction of four dimensional (4D) PET using phase-correlated 4D-computed tomography. *Phys Med Biol* 2008; **53**:N259–N268.

19 Visvikis D, Barret O, Fryer TD, Lamare F, Turzo A, Bizais Y, Le Rest CC. Evaluation of respiratory motion effects in comparison with other parameters affecting PET image quality. Nuclear Science Symposium Conference Record 2004 IEEE; 16–22 October 2004; Rome, Italy; Vol. 6. pp. 3668–3672.

20 Kinahan P, MacDonald L, Ng L, Alessio A, Segars P, Tsui B, Pathak S. Compensating for patient respiration in PET/CT imaging with the registered and summed phases (RASP) procedure. In: 3rd IEEE International Symposium on Biomedical Imaging: Nano to Macro; 6–9 April 2006; Arlington, VA. pp. 1104–1107.

21 Dawood M, Kösters T, Fieseler M, Büther F, Jiang X, Wübbeling F, Schäfers KP. Motion correction in respiratory gated cardiac PET/CT using multi-scale optical flow. *Med Image Comput Comput Assist Interv* 2008; **11 (Pt 2)**:155–162.

22 Qiao F, Pan T, Clark JW, Mawlawi OR. A motion-incorporated reconstruction method for gated PET studies. *Phys Med Biol* 2006; **51**:3769–3783.

23 Li T, Thorndyke B, Schreibmann E, Yang Y, Xing L. Model-based image reconstruction for four-dimensional PET. *Med Phys* 2006; **33**:1288.

24 Lamare F, Ledesma Carbayo MJ, Cresson T, Kontaxakis G, Santos A, Le Rest CC, *et al.* List-mode-based reconstruction for respiratory motion correction in PET using non-rigid body transformations. *Phys Med Biol* 2007; **52**:5187–5204.

25 Dawood M, Büther F, Lang N, Jiang X, Schaefers KP. Transforming static CT in gated PET/CT studies to multiple respiratory phases. Proceedings of the 18th International Conference on Pattern Recognition, Vol. 1; 20–24 August, 2006; Hong Kong. pp. 1026–1029.

26 Fayad H, Lamare F, Bettinardi V, Roux C, Visvikis D. Respiratory synchronized CT image generation from 40 PET acquisitions. In: IEEE Nuclear Science Symposium Conference Record; 19–25 October 2008; Dresden, Germany. pp. 5488–5492.

27 Wells RG, Ruddy TD, DeKemp RA, DaSilva JN, Beanlands RS. Single-phase CT aligned to gated PET for respiratory motion correction in cardiac PET/CT. *J Nucl Med* 2010; **51**:1182–1190.

28 McQuaid SJ, Lambrou T, Hutton BF. A novel method for incorporating respiratory-matched attenuation correction in the motion correction of cardiac PET-CT studies. *Phys Med Biol* 2011; **56**:2903–2915.

29 Seppenwoolde Y, Shirato H, Kitamura K, Shimizu S, van Herk M, Lebesque JV, Miyasaka K. Precise and real-time measurement of 3D tumor motion in lung due to breathing and heartbeat, measured during radiotherapy. *Int J Radiat Oncol Biol Phys* 2002; **53**:822–834.

30 George R, Vedam SS, Chung TD, Ramakrishnan V, Keall PJ. The application of the sinusoidal model to lung cancer patient respiratory motion. *Med Phys* 2005; **32**:2850–2861.

31 Nehmeh SA, Erdi YE, Pan T, Yorke E, Mageras GS, Rosenzweig KE, *et al*. Quantitation of respiratory motion during 4D-PET/CT acquisitions. *Med Phys* 2004; **31**:1333–1338.

32 Low DA, Nystrom M, Kalinin E, Parikh P, Dempsey JF, Bradley JD, *et al*. A method for the reconstruction of four-dimensional synchronized CT scans acquired during free breathing. *Med Phys* 2003; **30**:1254–1263.

33 McClelland JR, Blackall JM, Tarte S, Chandler AC, Hughes S, Ahmad S, *et al*. A continuous 4D motion model from multiple respiratory cycles for use in lung radiotherapy. *Med Phys* 2006; **33**:3348–3358.

34 Machac J, Bacharach SL, Bateman TM, Bax JJ, Beanlands R, Bengel F, *et al*. Positron emission tomography myocardial perfusion and glucose metabolism imaging. *J Nucl Cardiol* 2006; **13**:e121–e151.

35 Schleyer PJ, O'Doherty MJ, Barrington SF, Marsden PK. Retrospective data-driven respiratory gating for PET/CT. *Phys Med Biol* 2009; **54**:1935–1950.

36 Schleyer PJ, O'Doherty MJ, Marsden PK. Extension of a data-driven gating technique to 3D, whole body PET studies. *Phys Med Biol* 2011; **56**:3953–3965.

37 Dawood M, Büther F, Lang N, Schober O, Schäfers KP. Respiratory gating in positron emission tomography: a quantitative comparison of different gating schemes. *Med Phys* 2007; **34**:3067–3076.

38 Modat M, Ridgway GR, Taylor ZA, Lehmann M, Barnes J, Hawkes DJ, *et al*. Fast free-form deformation using graphics processing units. *Comput Methods Programs Biomed* 2010; **98**:278–284.

39 Rueckert D, Sonoda LI, Hayes C, Hill DLG, Leach MO, Hawkes DJ. Nonrigid registration using free-form deformations: application to breast MR images. *IEEE Trans Med Imaging* 1999; **18**:712–721.

40 Liu C, Pierce LA, Alessio AM, Kinahan PE. The impact of respiratory motion on tumor quantification and delineation in static PET/CT imaging. *Phys Med Biol* 2009; **54**:7345–7362.

41 Zeng R, Fessler JA, Balter JM, Balter PA. Iterative sorting for four-dimensional CT images based on internal anatomy motion. *Med Phys* 2008; **35**:917–926.

42 Wu H, Zhao Q, Berbeco RI, Nishioka S, Shirato H, Jiang SB. Gating based on internal/external signals with dynamic correlation updates. *Phys Med Biol* 2008; **53**:7137–7150.

43 Li R, Lewis JH, Cerviño LI, Jiang SB. 4D CT sorting based on patient internal anatomy. *Phys Med Biol* 2009; **54**:4821–4833.

44 Carnes G, Gaede S, Yu E, Van Dyk J, Battista J, Lee T-Y. A fully automated non-external marker 4D-CT sorting algorithm using a serial cine scanning protocol. *Phys Med Biol* 2009; **54**:2049–2066.

45 Thielemans K, Rathore S, Engbrant F, Razifar P. Device-less gating for PET/CT using PCA. In: Nuclear Science Symposium and Medical Imaging Conference (NSS/MIC), 2011 IEEE; 23–29 Oct 2011; Valencia, Spain. pp. 3904–3910.

46 Alessio AM, Kinahan PE, Champley KM, Caldwell JH. Attenuation-emission alignment in cardiac PET/CT based on consistency conditions. *Med Phys* 2010; **37**:1191–1200.

47 Manjeshwar R, Tao X, Asma E, Thielemans K. Motion compensated image reconstruction of respiratory gated PET/CT. In: 3rd IEEE International Symposium on Biomedical Imaging: Nano to Macro; 6–9 April 2006; Arlington, VA. pp. 674–677.

48 Polycarpou I, Tsoumpas C, Marsden PK. Statistical evaluation of PET motion correction methods using MR derived motion fields. 2011 IEEE Nuclear Science Symposium Conference Record; 23–29 October 2011; Valencia, Spain. pp. 3579–3585.

49 Bai W, Brady M. Motion correction and attenuation correction for respiratory gated PET images. *IEEE Trans Med Imaging* 2011; **30**:351–365.